Noncoherent Backscatter Communications over Ambient OFDM Signals

Mohamed A. ElMossallamy, *Student Member, IEEE,* Miao Pan, *Senior Member, IEEE,* Riku Jäntti, *Senior Member, IEEE,* Karim G. Seddik, *Senior Member, IEEE,* Geoffrey Ye Li, *Fellow, IEEE,* Zhu Han, *Fellow, IEEE*

Abstract—In recent years, ambient backscatter communications have gained a lot of interests as a promising enabling technology for Internet-of-Things and green communications. In ambient backscatter communication systems, ultra-low power devices are able to transmit information by backscattering ambient RF signals generated by legacy communication systems, such as Wi-Fi and cellular networks. This paper is concerned with ambient backscatter communications over legacy OFDM signals. We propose a backscatter modulation scheme that allows backscattering devices to take advantage of the spectrum structure of ambient OFDM symbols to transmit information. The proposed modulation scheme allows both binary and higher-order modulation using noncoherent energy detection. We investigate the detector design and analyze the error performance of the proposed scheme. We provide an exact expression for the error probability for the binary case, whereas accurate approximate expressions for the error probability are derived for the M-ary case. We corroborate our analysis using Monte-Carlo simulation and investigate the effects of varying the OFDM symbol size, maximum channel delay spread, and the number of receive antennas on the error performance. Our numerical results show that the proposed technique outperforms other techniques available in the literature for backscatter communication over ambient OFDM signals in different scenarios.

Index Terms—Ambient backscatter, Internet of things, green communications, RF-powered, wireless-powered.

I. INTRODUCTION

AMBIENT backscatter is a new paradigm that turns ambient radio-frequency (RF) signals from a source of interference to an opportunity for ultra-low power pervasive communications. Traditional backscatter is a mature technology [1] that has been used for many years to achieve short-range communications in power-constrained scenarios (e.g. RFID) [2]. In traditional backscatter communication systems, a dedicated device has to generate a continuous sinusoidal signal, which is phase-shifted and backscattered by tags by intentionally changing their antenna impedance to transmit information back to a reader device. However, in ambient backscatter, ambient RF transmission, which is vastly available (e.g. TV broadcast, cellular or Wi-Fi), is used instead of requiring the transmission of a dedicated sinusoidal signal. This makes ambient backscatter an attractive candidate for pervasive ultra-low power wireless networks.

The idea of ambient backscatter has been first introduced in [3], where ambient digital TV signals have been used to establish communication between two passive[1] tags in a device-to-device (D2D) manner. A simple prototype has been developed to demonstrate transmission with rates up to 1 Kbps over a somewhat modest communication range of 2.5 feet. Subsequently transmission rates and communication range have been significantly improved. In [4], Internet connectivity to battery-less RF-powered devices can be provided using two off-the-shelf commercial Wi-Fi access points (APs). Uplink rates of up to 1 kbps and a communication range of up to 2 meters have been achieved by modulating the channel state information (CSI) and received signal strength indicator (RSSI) signals in the WiFi packets. Downlink rates of up to 20 kbps and a communication range of up to 3 meters have been reached by using a clear-to-send-to-self (CTS-to-self) packet to silence other devices and then information is encoded in short WiFi packets (i.e. '1': send packet, '0': remain silent). The technique in [5] can achieve data rates of up to 1 Mbps and a communication range of 25 meters between two battery-less devices, which is made possible by two improvements over [3]: (1) direct-link (i.e. legacy-transmitter to reader) interference cancellation, and (2) orthogonal coding similar to CDMA chip sequences. Later in [6], rates of up to 5 Mbps and a communication range of up to 5 meters can be reached between a battery-less tag and a WiFi AP by using full-duplex radio and advanced self-interference cancellation techniques. Moreover, it has been demonstrated in [7] that WiFi packets can be synthesized by backscattering Bluetooth Low Energy (BLE) signals. More recently, in [8], 17 ambient signal sources spanning frequencies from 80 MHz up to 900 MHz were used, simultaneously, to achieve data rates of up to 1 kbps at distances up to 50 meters even when ambient carriers' powers were as low as -80 dBm.

More theoretical aspects of ambient backscatter communications such as derivation of error rates, information theoretic limits, and optimal scheduling were studied in [9]–[27]. In [9], it has been shown that the achievable sum rate of a communication system consisting of legacy MIMO nodes

Mohamed A. ElMossallamy, Miao Pan and Zhu Han are with the Electrical and Computer Engineering Department, University of Houston, TX, USA. Zhu Han is also with the Department of Computer Science and Engineering, Kyung Hee University, Seoul, South Korea.

Riku Jäntti is with the Department of Communications and Networking, Aalto University, Espoo, Finland.

Karim G. Seddik is with the Electronics and Communications Engineering Department, American University in Cairo, New Cairo, Egypt.

Geoffrey Ye Li is with the School of Electrical and Computer Engineering, Georgia Institute of Technology, Atlanta, GA, USA.

[1]In the literature, the tags are said to be passive if they do not posses traditional power-hungry active RF chains.

and backscattering nodes is more than what can be achieved by the legacy system alone. In [10], signal detection and error performance of an ambient backscatter communication system have been investigated where the tag uses a differential encoder to exempt the reader from estimating the channel, and an averaging technique, similar to the prototype in [3], is used for detection. The same approach has been extended to the case when the reader has multiple antennas in [13], where no specific modulation scheme is assumed for the legacy communication system, while simulations results following the same approach but using ambient WiFi transmissions can be found in [14]. In [17], differential Manchester encoding at the tag has been proposed to allow for differential detection without a threshold, while in [18], analytical expressions for the average error probability over flat Rayleigh fading channels have been derived. Moreover, the performance of a cooperative scheme where the receiver recovers information from both the ambient signal and the backscattered tag signal using successive interference cancellation (SIC) detectors has been investigated in [19]. Furthermore, the use of learning based clustering has been proposed in [20] to facilitate noncoherent detection. Finally, aspects related to resource allocation and scheduling in the context of ambient backscatter have been studied in [21]–[23], and a comprehensive survey can be found in [24].

Motivated by the fact that Orthogonal Frequency Division Multiplexing (OFDM) is the prevalent modulation scheme in most modern communications systems (e.g. DVB, LTE, WiFi), backscatter communications over ambient OFDM carrier signals has been studied in [26]–[28]. In [26], by taking advantage of the structure of the OFDM symbol in the time-domain, a modulation scheme for the ambient backscatter system has been designed, which canceled direct-link interference using the remaining part of the cyclic prefix, but required the reader to have knowledge of the relevant channels' lengths that have to be significantly shorter than the delay spread. Moreover, the fundamental information-theoretic limits of backscatter communication over ambient OFDM carriers, such as ergodic and outage capacity, have been investigated in [27]. It has been shown that ambient backscatter not only allows a battery-less tag to opportunistically communicate at satisfactory rates over short distances, but can also benefit legacy transmission by offering a form of diversity. In [28], a multi-antenna receiver backscatter receiver that relied only on the statistical properties of OFDM signals has been proposed.

In this paper, we investigate backscatter communications over ambient OFDM signals exploiting null subcarriers extending the work that we first presented in [29]. Our contributions in this paper can be summarized as follows:

- We propose a modulation scheme for backscatter communications over ambient OFDM carriers taking advantage of the in-band null subcarriers. We design the tag modulation waveform for the binary case and the detector to avoid direct-link interference.
- We analyze the error performance of the proposed scheme and obtain an exact expression for the average error probability in terms of the bivariate Meijer G-function. Different from [10], [12], [26], we do not use Gaussian

approximations and our analysis takes into account the cascaded fading nature of the backscatter channel and the correlations inherent in the OFDM waveform and the wideband wireless channel.

- To improve error performance, we propose using multiple receive antennas. In particular, we propose using noncoherent *post-detection* Equal Gain Combining, to get composite test statistics for energy detection without knowledge of the channel realization or the ambient OFDM symbol. We extend our error analysis to the case of multiple receive antennas and obtain an exact expression for the error probability.
- To improve the communication rate, building on the same basic idea of shifting energy to null subcarriers, we propose an M-ary modulation scheme allowing the transmission of multiple bits per OFDM symbol while retaining the ability to be detected noncoherently, relying only on energy detection. We model the M-ary detection as traditional detection over a general vector channel problem and obtain accurate approximate error probability expressions.
- Finally, we provide simulation results to corroborate our analysis and to study the effects of multiple system parameters, namely, the maximum channel delay spread, OFDM symbol size, and number of receive antennas, on the error performance of the proposed modulation scheme.

The rest of the paper is organized as follows. In Section II, we present the system model. In Section III, we introduce our modulation scheme for backscatter communications over ambient OFDM signals and investigate the error performance of our scheme. In Section IV, we extend our analysis to the case of multiple antennas at the reader. In Section V, we extend our scheme to support M-ary modulation and analyze the error performance in that case. In Section VI, we present simulation results to corroborate our analysis, compare our scheme to the existing schemes in the literature and study the effects of multiple system parameters on the error performance. Finally, in Section VII, we conclude the paper.

II. SYSTEM MODEL

In general, we have two co-existing communications systems as in Fig. 1. A legacy communication system that employs OFDM, e.g. LTE, and a capillary ambient backscatter communication system consisting of ultra-low power tags/sensor nodes and readers. The legacy nodes are not power-constrained and are either powered by large-capacity batteries (e.g. user equipment) or the power-grid (e.g. base stations) while the capillary tags/sensor nodes may rely on RF-energy harvesting [30] for power and can only communicate by rescattering the legacy system OFDM transmission. The readers can either be independent devices or part of the legacy nodes [27].

Next, we assume there are one legacy transmitter, one tag, and one reader. The legacy transmitter and the tag have a single antenna each, while the reader has R receiving antennas. The tag modulates its information into the ambient OFDM signal by intentionally altering its antenna impedance to phase-shift
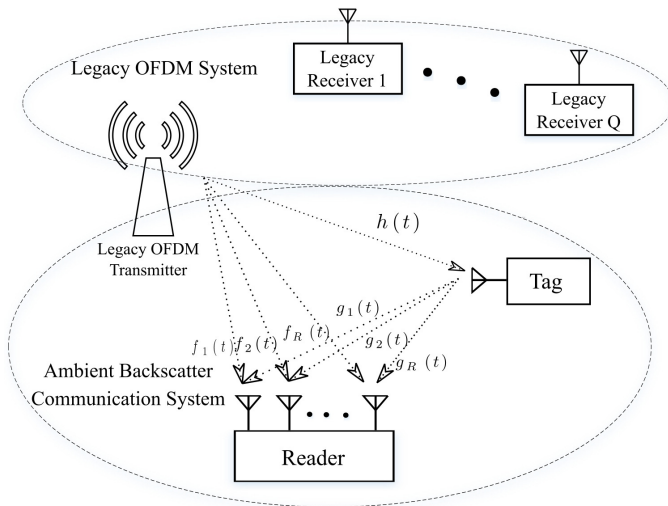
Fig. 1. System Model

and rescatter the ambient signal so that the reader can decode the information by observing the difference in received energy. Hence, the tag does not require any power-hungry RF chains for communications and may be powered by an RF-energy harvester.

As shown in Fig. 1, let $h(t)$, $f_r(t)$ and $g_r(t)$ denote, respectively, the bandpass impulse responses of the multipath Rayleigh fading channels between the legacy transmitter and the tag, the legacy transmitter and the r-th reader antenna, and the tag and the r-th reader antenna. The multi-path delay spreads corresponding to these channels are denoted, respectively, by τ_h, τ_{f_r} and τ_{g_r}. All channels are assumed to be mutually independent.

Denote the bandpass signal transmitted from the OFDM legacy transmitter during a symbol interval as

$$s(t) = \Re\left\{ \sqrt{p}\ s_l(t)\, \mathrm{e}^{j2\pi f_c t} \right\}, \qquad (1)$$

where p is the average transmitted power, $s_l(t)$ is the baseband representation of $s(t)$, and f_c is the carrier frequency. The received signal at the tag can be written as

$$x(t) = \Re\left\{ \left[\sqrt{p}\ s_l(t) * h(t) \right] \mathrm{e}^{j2\pi f_c t} \right\}, \qquad (2)$$

where $*$ denote linear convolution and $x_l(t) = \sqrt{p}s_l(t) * h_l(t)$ is the baseband representation of $x(t)$.

The tag modulates its information onto the received signal by changing its antenna impedance. Let $b_l(t)$ denote the baseband representation of the tag's modulation waveform with corresponding bandpass signal $b(t)$. As in the literature on ambient backscatter communications [10], [12], [13], [26], we assume that no noise is added at the tag. This assumption arises from the fact that the tag does not use any active RF components. Thus, the signal backscattered from the tag will be $x(t)b(t)$.

The received signal at the r-th reader antenna can be written as

$$y_r(t) = \underbrace{[x(t)b(t)] * g_r(t)}_{y_r^b(t)} + \underbrace{s(t) * f_r(t)}_{y_r^d(t)} + w_r(t), \qquad (3)$$

where $y_r^b(t) = [x(t)b(t)] * g_r(t)$ is the signal backscattered from the tag, $y_r^d(t) = \sqrt{p}s(t) * f_r(t)$ is the signal received directly from the legacy transmitter and $w_r(t)$ is the bandpass "white" Gaussian noise random process, which is independent of both $y_r^b(t)$ and $y_r^d(t)$. Note that tag's information in present only in the term $y_r^b(t)$, while the term $y_r^d(t)$ is the direct-link (i.e. legacy-transmitter to reader) interference and is independent from the tag's information. The baseband representation of (3) can be written as

$$y_{r,l}(t) = y_{r,l}^b(t) + y_{r,l}^d(t) + w_{r,l}(t), \qquad (4)$$

where $y_{r,l}^b(t)$, $y_{r,l}^d(t)$, and $w_{r,l}(t)$ denote the baseband representations of $y_r^b(t)$, $y_r^d(t)$, and $w_r(t)$, respectively.

At the reader, the received signal is down-converted to baseband and passed through an analog-to-digital converter (ADC). The resultant discrete-time baseband sequence, for one OFDM symbol before discarding the cyclic prefix, can be written as

$$y_{r,l}[n] = y_{r,l}^b[n] + y_{r,l}^d[n] + w_{r,l}[n], \quad n = 1, \ldots, N_f + N_{cp}, \qquad (5)$$

where N_f is the number of subcarriers, or equivalently the length of the fast Fourier transform (FFT), N_{cp} is the cyclic prefix length, and $w_{r,l}[n]$ is complex baseband additive white Gaussian noise (AWGN) with zero-mean and variance $\sigma_w^2 \ \forall \ r \in \{1, 2, \ldots, R\}$. Let $h_l[n]$, $f_{r,l}[n]$, and $g_{r,l}[n]$ denote the discrete-time baseband representation of $h(t)$, $f_r(t)$ and $g_r(t)$, respectively. Hence, we can write $y_{r,l}^b[n] = (x_l[n] b_l[n]) * g_{r,l}[n]$ and $y_{r,l}^d[n] = \sqrt{p}s_l[n] * f_l[n]$. The discrete-time channels' lengths are given by $L_h = \lfloor \tau_h f_s \rfloor$, $L_{f_r} = \lfloor \tau_{f_r} f_s \rfloor$ and $L_{g_r} = \lfloor \tau_{g_r} f_s \rfloor$, where f_s is the sampling frequency. Let $\tau_r \triangleq \max\{\tau_{f_r}, \tau_h + \tau_{g_r}\}$ denote the maximum channel delay spread seen by the r-th reader antenna; hence, $L_r \triangleq \max\{L_{f_r}, L_h + L_{g_r} - 1\}$ denote the discrete-time length of maximum channel delay spread seen by the r-th reader antenna. For simplicity and without loss of generality, assume all receive antennas see the same delay spread and denote it by τ. Finally, since the distance between the tag and reader is fairly small in practice, it is reasonable to assume that $L_{g_r} = 1 \ \forall \ r \in \{1, 2, \ldots, R\}$. Hence, the backscattered signal at the reader can be simplified to $y_{r,l}^b[n] = g_r x_l[n] b_l[n]$, where g_r is the complex flat fading channel gain between the tag and the r-th reader's antennas. In the rest of the paper, we use the discrete-time baseband model and drop the subscript l for notational convenience.

Our goal is to design the tag modulation waveform $b[n]$ and the detector at the reader to be able to extract the tag information in $b[n]$ from the received signal $\{y[n]\}_{r=1}^R$ without knowing either the transmitted OFDM symbol $s[n]$ or the relevant channels $h[n]$, $\{f_r[n]\}_{r=1}^R$, and $\{g_r\}_{r=1}^R$.

III. SINGLE-ANTENNA TRANSCEIVER DESIGN AND PERFORMANCE ANALYSIS

In this section, we propose a modulation scheme for backscatter communications over ambient OFDM signals. We describe the tag modulation waveform and study the detector design in Section III-A. We also analyze the error performance of the proposed scheme and obtain exact expressions for the

error probability in Section III-B. We restrict ourselves to the case of a single-antenna receiver in this section and address the multiple antennas case in the next section.

A. Backscatter Waveform Design

In OFDM systems, the edge subcarriers are usually left null. For example, in the LTE standard, for the 10 MHz carrier, the number of subcarriers is 1024, out of which 423 subcarriers are left null [31]. A portion of these null subcarriers fall inside the 10 MHz channel bandwidth and were originally conceived to serve as a guard band. Recently, this guard band was proposed as one of the deployment options for NB-IoT [32]. It was found in [33], that even for active NB-IoT transceivers interference effects were minimal. This makes the guard band a great candidate for Ambient Backscatter.[2] Let $\mathcal{U}$ denote the set of in-band null subcarriers.

We exploit the structure of the OFDM symbol spectrum by designing the tag modulation waveform $b[n]$ to shift the backscattered energy into these null subcarriers so that a simple energy detector can be used to decode the tag information. This exempts the reader from knowing the transmitted OFDM symbol or any of the relevant channels. Similar to [26], [27], we assume the tag is synchronized to the ambient OFDM signal and that every backscatter symbol spans the duration of one legacy OFDM symbol. The tag uses the following waveform to convey one information bit per OFDM symbol

$$b[n] \triangleq e^{i\pi Bn}, \quad n = 1, 2, \ldots, N_f + N_{cp}, \qquad (6)$$

where $B \in \{0, 1\}$ is the information bit being transmitted. Hence, to transmit a '1' bit the tag will alternate its antenna impedance between two states, one state causes a phase shift of π and the other state provides no phase shift while to transmit a '0' bit the tag keeps its antenna impedance constant at a value that provides no phase shift. Using this tag waveform, the backscattered signal received at the reader can be written as

$$y^b[n] = g\, x[n]\, e^{i\pi Bn}. \qquad (7)$$

Taking the discrete Fourier transform of (7), the backscattered signal spectrum can be written as

$$Y^b[m] = gX[m] \circledast \delta\left[m - \frac{Bf_s}{2}\right] = g\, X\left[m - \frac{Bf_s}{2}\right], \qquad (8)$$

where $\circledast$ denotes circular convolution and $X[m]$ is the discrete Fourier transform (DFT) of $x[n]$. Thus, from the viewpoint of the frequency domain, to transmit a '1' bit, the tag shifts the spectrum of the backscattered signal. This shift in frequency will cause a large fraction of the backscattered energy to fall into all the null subcarriers. Hence, an energy detector over the null subcarriers can be used at the receiver to decode the tag information.

B. Detector

In this subsection, we design the detector for the modulation scheme introduced the previous subsection. The reader only knows the set of in-band null subcarriers, $\mathcal{U}$, along the edges of the ambient OFDM symbol and the average signal to noise ratio (SNR), but has no knowledge of the OFDM ambient signal, $s[n]$, or the relevant channels $h[n]$, $f[n]$ or g. Since the tag transmits its information by shifting the spectrum of the backscattered signal into the null subcarriers, an energy detector is used to collect the energy in the null subcarriers, and decode the tags information. However, only null subcarriers inside channel bandwidth can be used for energy detection, since those outside the channel bandwidth may be subject to adjacent channel interference. Hence, in the rest of the paper, we are only concerned with the set of in-band null subcarriers.

Decision Statistics: At the reader, the cyclic prefix is discarded, and the remaining N_f samples are passed through an FFT block. Let $Y[m]$ denote the output of the FFT. Hence, the test statistic can be written as

$$z = \frac{2}{\sigma_w^2} \sum_{m \in \mathcal{U}} |Y[m]|^2. \qquad (9)$$

Under $\mathcal{H}_0$, the hypothesis that the tag transmitted a '0' bit, the null subcarriers contain only noise[3] and z is the sum of the squares of $2|\mathcal{U}|$ standard Gaussian random variables. Hence, $p(z|B = 0)$ is a central Chi-squared distribution with $2|\mathcal{U}|$ degrees of freedom [34]. On the other hand, when the tag is transmitting a '1' bit, the distribution of the decision statistics z is fairly complicated. Under $\mathcal{H}_1$, the hypothesis that the transmitted bit is '1', the received energy in the null subcarriers depends on the random channels g and $h[n]$. Therefore, the instantaneous detection SNR is a random variable and can be written as

$$\gamma = \frac{p|g|^2 \sum_{m \in \mathcal{U}} |H[m]|^2}{|\mathcal{U}|\sigma_w^2}, \qquad (10)$$

where $\{H[m]\}_{m \in \mathcal{U}}$ are the flat-fading channel coefficients seen by the in-band null-subcarriers. Note that the channel gains on adjacent subcarriers will be necessarily correlated. This correlation arises from the fact that in all OFDM systems, subcarrier spacing has to be chosen to be smaller than the channel coherence bandwidth to ensure each subcarrier sees a flat channel and no cumbersome equalization is required. Let $\mathbf{h}$ denote the vector comprising the channel coefficients $\{H[m]\}_{m \in \mathcal{U}}$, and $\mathbf{R}_H = E\left[\mathbf{h}\mathbf{h}^\dagger\right]$ the corresponding covariance matrix.

Theorem 1. The distribution of the instantaneous detection SNR, γ, for the single-antenna receiver is given by

$$f(\gamma) = \sum_{j=1}^{J} \left(\prod_{k \neq j} \frac{\frac{1}{\lambda_k}}{\frac{1}{\lambda_k} - \frac{1}{\lambda_j}} \right) \frac{1}{\gamma} G_{0,2}^{2,0} \left(\left. \frac{}{1,1} \right| \frac{|\mathcal{U}|\, \gamma}{\lambda_j\, \overline{\gamma}} \right), \qquad (11)$$

where $\{\lambda_j\}_{j=1}^{J}$ are the non-zero eigenvalues of the co-variance matrix $\mathbf{R}_H = E\left[\mathbf{h}\mathbf{h}^\dagger\right]$, and $G_{\cdot,\cdot}^{\cdot,\cdot}(\cdot|\cdot)$ is the Meijer G-function

---

[2]Note that ambient backscatter devices do not possess traditional wireless transmitters with power amplifiers, and the backscattered energy is limited in range and too minuscule compared to traditional transmitters making interference with adjacent transmissions insignificant.

[3]We assume ICI is negligible since (1) the tag, reader and legacy transmitter are stationary, (2) at practical low-medium SNRs, noise is dominant. (3) ICI is weakest at edge subcarriers.
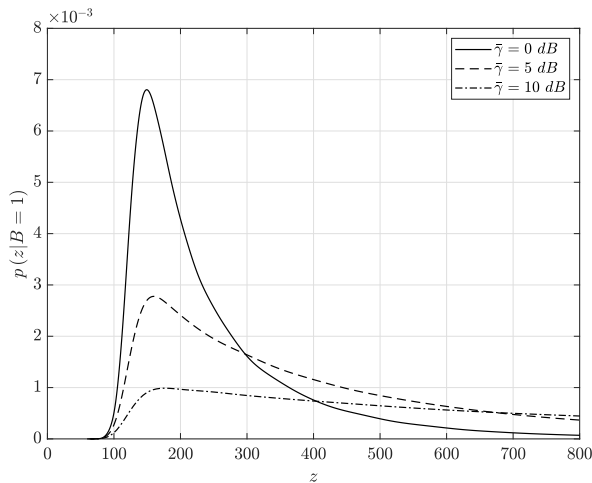
Fig. 2. Probability distribution function of the test statitsic z under $\mathcal{H}_1$ for different values of SNR. $N_f = 1024, |\mathcal{U}| = 66, \tau = 3\mu s, L_g = 1$.

[35].

Proof. See Appendix A. □

The expression for the distribution of the SNR obtained in Theorem 1 will be essential in computing the distribution of test statistics and the average probability of error.

Conditional on the instantaneous received SNR, γ, the decision statistic distribution $p(z|\gamma, B = 1)$ is a noncentral Chi-squared with $2|\mathcal{U}|$ degrees of freedom and noncentrality parameter $2|\mathcal{U}|\gamma$ [34].

Proposition 1. The distribution of the decision statistic, z, under $\mathcal{H}_1$ is given by

$$p(z|B=1) = \sum_{j=1}^{J} \pi \left(\prod_{k \neq j} \frac{\frac{1}{\lambda_k}}{\frac{1}{\lambda_k} - \frac{1}{\lambda_j}} \right) \left(\frac{z}{2} \right)^{|\mathcal{U}|-1} e^{-\frac{z}{2}}$$
$$\times G_{1,0:0,2:1,3}^{1,0:2,0:1,0} \left(0 \left| \begin{matrix} - \\ 1,1 \end{matrix} \right| \begin{matrix} \frac{1}{2} \\ 0, 1 - |\mathcal{U}|, \frac{1}{2} \end{matrix} \left| \frac{1}{\lambda_j \overline{\gamma}}, \frac{z}{2} \right. \right). \tag{12}$$

Proof. The distribution is found by averaging the noncentral Chi-squared distribution over the distribution of the instantaneous SNR obtained in Theorem 1. See Appendix B for details. □

The bivariate Meijer G-function is not available as a built-in function in well-known computational software packages (e.g. MATLAB, Wolfram Mathematica, Maple); however, there exist two implementations in the literature, using Wolfram Mathematica in [36], and MATLAB in [37]. Fig. 2 shows how $p(z|B = 1)$ looks for different values of SNR. Note that increasing the SNR increases both the mean and variance of the test statistic, which leads to slowly-decaying tails. Finally, note that this proposed scheme does not suffer from direct link interference at the reader as the energy from the direct link exists only on the data subcarriers.

Error Performance: Next, we analyze the probability of error for the proposed scheme. Let δ denote the decision threshold. Then, since the tag transmitted bits are equally probable to be ones or zeros, the average probability of error is given by

$$P_e(\delta) = \frac{1}{2} P_{e|B=0}(\delta) + \frac{1}{2} P_{e|B=1}(\delta). \tag{13}$$

Both $P_{e|B=0}(\delta) = Pr(\hat{B} = 1|B = 0)$ and $P_{e|B=1}(\delta) = Pr(\hat{B} = 0|B = 1)$ are functions of the decision threshold δ, which should be optimized to minimize the average probability of error $P_e(\delta)$. $P_{e|B=0}(\delta)$ is independent of the SNR and is given by the tail probability of the central Chi-squared distribution as [38]

$$P_{e|B=0}(\delta) = \frac{\Gamma\left(|\mathcal{U}|, \frac{\delta}{2}\right)}{\Gamma(|\mathcal{U}|)}, \tag{14}$$

where $\Gamma(s, x) = \int_x^\infty t^{s-1} e^{-t} dt$ is the *upper* incomplete Gamma function, and $\Gamma(s) = \int_0^\infty t^{s-1} e^{-t} dt$ is the "complete" Gamma function. Whereas, $P_{e|B=1}(\delta)$ is dependent on the instantaneous SNR and subsequently on the random backscatter channel. We can write $P_{e|B=1}(\delta)$, conditional on the instantaneous SNR, using the cumulative distribution function (CDF) of the noncentral Chi-squared random variable as

$$P_{e|\gamma, B=1}(\delta) = 1 - Q_{|\mathcal{U}|}\left(\sqrt{2|\mathcal{U}|\gamma}, \sqrt{\delta}\right), \tag{15}$$

where $Q_{\cdot}(\cdot, \cdot)$ is the Marcum Q-Function. Thus, using (11), we can average $P_{e|\gamma, B=1}(\delta)$ over the distribution of the instantaneous SNR to obtain (16).

$$P_{e|B=1}(\delta) = 1 - \sum_{j=1}^{J} \left(\prod_{k \neq j} \frac{\frac{1}{\lambda_k}}{\frac{1}{\lambda_k} - \frac{1}{\lambda_j}} \right) \int_0^\infty \gamma^{-1}$$
$$\times Q_{|\mathcal{U}|}\left(\sqrt{2|\mathcal{U}|\gamma}, \sqrt{\delta}\right) G_{0,2}^{2,0}\left(\left. \begin{matrix} - \\ 1,1 \end{matrix} \right| \frac{|\mathcal{U}|}{\lambda_j} \frac{\gamma}{\overline{\gamma}} \right) d\gamma. \tag{16}$$

Using Theorem 1 in [39], the integral in (16) can be evaluated in terms of the bivariate Meijer G-function [40]. Hence, we can write the average probability of error as a function of the threshold as in (17)

$$P_e(\delta) = \frac{1}{2} + \frac{\Gamma\left(|\mathcal{U}|, \frac{\delta}{2}\right)}{2\Gamma(|\mathcal{U}|)} + \sum_{j=1}^{J} \frac{1}{2\lambda_j \overline{\gamma}} \left(\prod_{k \neq j} \frac{\frac{1}{\lambda_k}}{\frac{1}{\lambda_k} - \frac{1}{\lambda_j}} \right)$$
$$\times G_{1,0:1,3:1,3}^{0,1:1,0:2,1}\left(0 \left| \begin{matrix} \frac{1}{2} \\ 0, -|\mathcal{U}|, \frac{1}{2} \end{matrix} \right| \begin{matrix} 1 \\ 1,1,0 \end{matrix} \left| \frac{\sqrt{\delta}}{2}, \frac{1}{\lambda_j \overline{\gamma}} \right. \right). \tag{17}$$

Detector Threshold: The decision threshold should be chosen to minimize the average probability of error in (17), i.e.

$$\delta^* = \arg\min_\delta P_e(\delta). \tag{18}$$

Since the tag transmits ones and zeros with equal probability, the optimal decision rule that minimizes the probability of error is the maximum likelihood (ML) rule [41] given by

$$\hat{B} = \begin{cases} 1, & p(z|B = 1) \geq p(z|B = 0), \\ 0, & p(z|B = 0) > p(z|B = 1). \end{cases} \tag{19}$$

Hence, the optimal decision threshold, δ^*, lies at the intersection of the two likelihood functions, $p\left(z|B=0\right)$ and $p\left(z|B=1\right)$. Unfortunately, a closed-form expression for δ^* cannot be found analytically. However, it can be easily found numerically, for any SNR, using a simple, one-dimensional line search.

IV. MULTI-ANTENNA RECEIVER DESIGN AND PERFORMANCE ANALYSIS

In this section, we extend the analysis carried out in the previous section to the case where the reader possesses multiple antennas. The same backscatter waveform design described in Section III-A is used at the tag. We construct composite test statistics from the signals received on all reader's antennas and analyze the distribution of the test statistic and error performance of the proposed scheme in the case of multiple antennas.

A. Decision Statistic

As we mentioned in Section II, we assume the backscatter receiver is unable to obtain knowledge of the transmitted ambient OFDM signal $s\left[n\right]$ or the relevant channels $h\left[n\right], \{f_r\left[n\right]\}_{r=1}^{R}$, and $\{g_r\}_{r=1}^{R}$. Hence, diversity combining must be done noncoherently. Thus, we use noncoherent post-detection Equal Gain Combining (EGC), which is also referred to as square-law combining [42, Sec. 9.4].

For the r-th antenna in the backscatter receiver, we construct the following test statistic

$$z_r = \frac{2}{\sigma_w^2} \sum_{m\in\mathcal{U}} |Y_r\left[m\right]|^2, \qquad (20)$$

where $Y_r\left[m\right]$ is the output of the FFT at the r-th antenna. The distribution of (20) has been discussed in Section III. Next, we combine the test statistics at the R antennas with equal weights and get the composite test statistic

$$z_c = \sum_{r=1}^{R} z_r = \frac{2}{\sigma_w^2} \sum_{r=1}^{R} \sum_{m\in\mathcal{U}} |Y_r\left[m\right]|^2. \qquad (21)$$

Next, we study the distribution of the composite test statistics under both hypotheses, $\mathcal{H}_0$ and $\mathcal{H}_1$. Under $\mathcal{H}_0$, z_c is the sum of R independent central Chi-squared random variables with $2|\mathcal{U}|$ degrees of freedom each, where independence follows from the fact that noise at different receive antennas are independent. Hence, z_c under $\mathcal{H}_0$ follows a central Chi-squared distribution with $2R|\mathcal{U}|$ degrees of freedom.

On the other hand, the distribution of composite test statistics under $\mathcal{H}_1$ depends on the random backscatter channels. As we did in the single-antenna case, we first consider the conditional distribution for a given received instantaneous SNR at the output of the combiner, γ_c. We assume all receive antennas have the same average SNR. In that case, the distribution is a noncentral Chi-squared with $2R|\mathcal{U}|$ degrees of freedom, and a noncentrality parameter given by $2|\mathcal{U}|\gamma_c$, where $\gamma_c = \sum_{r=1}^{R} \gamma_r$ is the sum of the SNRs at all receive antennas. Each γ_r is a random variable whose distribution is

given by (40) and whose expected value is $E\left[\gamma_r\right] = \overline{\gamma}$. The combined instantaneous SNR, γ_c, can be written as

$$\gamma_c = \frac{p}{|\mathcal{U}|\sigma_w^2} \sum_{r=1}^{R} |g_r|^2 \sum_{m\in\mathcal{U}} |H\left[m\right]|^2. \qquad (22)$$

Theorem 2. The distribution of the instantaneous detection SNR, γ_c, at the output of the combiner for the multi-antenna receiver is given by

$$f\left(\gamma_c\right) = \frac{\gamma_c^{-1}}{(R-1)!} \sum_{j=1}^{J} \left(\prod_{k\neq j} \frac{\frac{1}{\lambda_k}}{\frac{1}{\lambda_k}-\frac{1}{\lambda_j}}\right) G_{0,2}^{2,0}\left(\left.\overline{R,1}\right| \frac{|\mathcal{U}|\gamma_c}{\lambda_j\overline{\gamma}}\right). \qquad (23)$$

where $\{\lambda_j\}_{j=1}^{J}$ are as defined earlier in (11).

Proof. See Appendix C. □

Similar to Section III-B, the distribution of the SNR at the output of the combiner, γ_c, obtained in Theorem 2 can be used to calculate the distribution of combiner test statistic, z_c, under $\mathcal{H}_1$, and the average probability of error.

Proposition 2. The distribution of the decision statistic at the output of the combiner, z_c, under $\mathcal{H}_1$ is given by

$$p\left(z_c|B=1\right) = \frac{\pi e^{-\frac{z_c}{2}}}{2\left(R-1\right)!} \left(\frac{z_c}{2}\right)^{R|\mathcal{U}|-1} \sum_{j=1}^{J} \left(\prod_{k\neq j} \frac{\frac{1}{\lambda_k}}{\frac{1}{\lambda_k}-\frac{1}{\lambda_j}}\right)$$
$$\times G_{1,0:0,2:1,3}^{1,0:2,0:1,0}\left(0 \left|\begin{array}{c} - \\ R,1 \end{array}\right| \begin{array}{c} \frac{1}{2} \\ 0,1-R|\mathcal{U}|,\frac{1}{2} \end{array}\left|\frac{1}{\lambda_j\overline{\gamma}},\frac{z_c}{2}\right.\right). \qquad (24)$$

Proof. The distribution is found by averaging the noncentral Chi-squared distribution over the distribution of the instantaneous SNR at the output of the combiner, γ_c, obtained in Theorem 2. See Appendix D for details □

B. Error Performance

Next, we analyze the probability of error for the multi-antenna receiver. Let δ denote the decision threshold. Assume tag transmitted bits are equally probable to be ones or zeros, then the average probability of error is given by

$$P_e\left(\delta\right) = \frac{1}{2} P_{e|B=0}\left(\delta\right) + \frac{1}{2} P_{e|B=1}\left(\delta\right). \qquad (25)$$

Similar to the single antenna case, both $P_{e|B=0}\left(\delta\right) = Pr(\hat{B}=1|B=0)$ and $P_{e|B=1}\left(\delta\right) = Pr(\hat{B}=0|B=1)$ are functions of the decision threshold δ, which should be chosen to minimize the average probability of error, $P_e\left(\delta\right)$. $P_{e|B=0}\left(\delta\right)$ is independent of the SNR and is given by the tail probability of the central Chi-squared distribution with $R|\mathcal{U}|$ degrees of freedom as

$$P_{e|B=0}\left(\delta\right) = \frac{\Gamma\left(R|\mathcal{U}|,\frac{\delta}{2}\right)}{\Gamma\left(R|\mathcal{U}|\right)}, \qquad (26)$$

whereas, $P_{e|B=1}\left(\delta\right)$ is dependent on the instantaneous SNR and subsequently on the random backscatter channel. We can write $P_{e|B=1}\left(\delta\right)$, conditional on the instantaneous SNR, using the CDF of the noncentral Chi-squared random variable as

$$P_{e|\gamma,B=1}\left(\delta\right) = 1 - Q_{R|\mathcal{U}|}\left(\sqrt{2|\mathcal{U}|\gamma_c},\sqrt{\delta}\right). \qquad (27)$$

Thus, using (45), we can average $P_{e|\gamma,B=1}(\delta)$ over the distribution of the instantaneous SNR to obtain

$$
\begin{aligned}
P_{e|B=1}(\delta) = 1 - \sum_{j=1}^{J} &\left(\prod_{k \neq j} \frac{\frac{1}{\lambda_k}}{\frac{1}{\lambda_k} - \frac{1}{\lambda_j}} \right) \int_0^\infty \gamma_c^{-1} \\
&\times Q_{R|\mathcal{U}|}\left(\sqrt{2|\mathcal{U}|\gamma_c}, \sqrt{\delta} \right) G_{0,2}^{2,0}\left(\left. \frac{}{R,1} \right| \frac{|\mathcal{U}|}{\lambda_j} \frac{\gamma_c}{\overline{\gamma}} \right) \mathrm{d}\gamma_c.
\end{aligned}
\tag{28}
$$

The integral in (28) is very similar to (16) and can be readily evaluated to yield the average error probability given by

$$
\begin{aligned}
P_e(\delta) = \frac{1}{2} + &\frac{\Gamma\left(R|\mathcal{U}|, \frac{\delta}{2}\right)}{2\Gamma(R|\mathcal{U}|)} + \frac{1}{2(R-1)!} \sum_{j=1}^{J} \frac{1}{\lambda_j \overline{\gamma}} \left(\prod_{k \neq j} \frac{\frac{1}{\lambda_k}}{\frac{1}{\lambda_k} - \frac{1}{\lambda_j}} \right) \\
&\times G_{1,0:1,3:1,3}^{0,1:1,0:2,1}\left(\left. \begin{matrix} 0 \\ - \end{matrix} \right| \left. \begin{matrix} \frac{1}{2} \\ 0, -R|\mathcal{U}|, \frac{1}{2} \end{matrix} \right| \left. \begin{matrix} 1 \\ R, 1, 0 \end{matrix} \right| \frac{\sqrt{\delta}}{2}, \frac{1}{\lambda_j \overline{\gamma}} \right).
\end{aligned}
\tag{29}
$$

V. HIGHER ORDER MODULATION

In this section, we extend the binary modulation scheme presented in Section III-A to allow sending more bits per tag symbol. In particular, we divide the set of in-band null subcarriers into different subsets and design the tag symbols to cause the backscattered energy to lay within specific subsets enabling the transmission of multiple bits per OFDM symbol.

A. Backscatter Waveform Design for Higher Order Modulation

Next, we describe the tag modulation waveform used for the M-ary case. The waveform for the m-th symbol can be written as

$$
b_m[n] \triangleq e^{i\pi\theta_m n}, \quad m = 0, 1, \ldots, M-1
\tag{30}
$$

where θ_m specifies the amount of frequency shift caused by the m-th symbol. To elaborate, the tag will change its antenna impedance to cause a specific sequence of phase shifts corresponding to a complex sinusoid with a particular frequency associated with the particular tag symbol being transmitted. The implementation of different phase shifts is a well studied problem in RFID [6], [43]. This allows us to shift the ambient OFDM signal into specific null subcarriers to implement higher order backscatter modulation that can be decoded noncoherently using only energy detection. The set of backscatter symbols can be constructed using the following two steps:

1) Given the number of bits to transmit per OFDM symbol, $k = \log_2 M$, divide the set of in-band null subcarriers, $\mathcal{U}$, into $2^k - 1$ contiguous subsets $\{\mathcal{U}_u\}_{u=1}^{2^k-1}$.
2) Set the amount of spectrum shift induced by each backscatter symbol, θ_m, such that θ_0 induces no shift, θ_1 shifts the ambient spectrum to only $\mathcal{U}_1$, θ_2 shifts the ambient spectrum to $\mathcal{U}_1 \cup \mathcal{U}_2$, and so on, up to θ_{M-1} shifts the ambient spectrum to $\cup_{u=1}^{u=M-1}\mathcal{U}_u$ [4]. The backscatter

---

Fig. 3. Probability distribution function of the test statistic z_c for different backscatter symbols from Example 1. $R = 8, \overline{\gamma} = 25$ dB. $N_f = 2048, |\mathcal{U}| = 132, \tau = 3\mu s$.

symbols $\{b_m\}_{m=0}^{M-1}$ follow directly from $\{\theta_m\}_{m=0}^{M-1}$ by substituting in (30).

We illustrate this construction by way of an example.

Example 1. Consider an ambient 20 MHz LTE carrier with 132 out of 847 null subcarriers in-band. Assume the tag send 2 bits per OFDM symbol. Hence, we have four symbols corresponding to four different levels of spectrum shifts $\{\theta_0, \theta_1, \theta_2, \theta_3\}$. Divide the set of in-band null subcarriers into three non-overlapping contiguous subsets, $\mathcal{U}_1$, $\mathcal{U}_2$ and $\mathcal{U}_3$, each containing 44 subcarriers. The phase shifts are designed such that the four symbols correspond to no spectrum shift, spectrum shift to $\mathcal{U}_1$, spectrum shift to $\mathcal{U}_1 \cup \mathcal{U}_2$, and spectrum shift to $\mathcal{U}_1 \cup \mathcal{U}_2 \cup \mathcal{U}_3$, respectively.

Using this construction, the tag symbols can be decoded at the receiver by observing the energy levels in different null subsets.

B. Detector for Higher-Order Modulation

Next, we explain how to decode the tag data. Using the same test statistics as in (9) to perform straight-forward multi-level energy detection would result in poor error performance under the fading conditions considered in the system model. Fig. 3 shows the distribution of the received energy over all the in-band null subcarriers, z_c, for the case in Example 1. As can be seen from Fig. 3, likelihoods of the received energy for different symbols have great overlap and distinguishing between different backscatter symbols using traditional multi-level energy detection would lead to an abysmal error performance, even at high SNRs and with a large number of antennas at the receiver. Hence, we propose an improved detection technique that relies on energy detection for each subset independently. Even if we cannot prove its optimality, our simulation results in Section VI will demonstrate its effectiveness.

---

[4]The reason for this construction is the fact that the number of data subcarriers exceeds the number of guard subcarriers; hence, a shift to $|\mathcal{U}_M|$ will necessarily shift energy to $\cup_{u=1}^{u=M-1}\mathcal{U}_u$ as well.
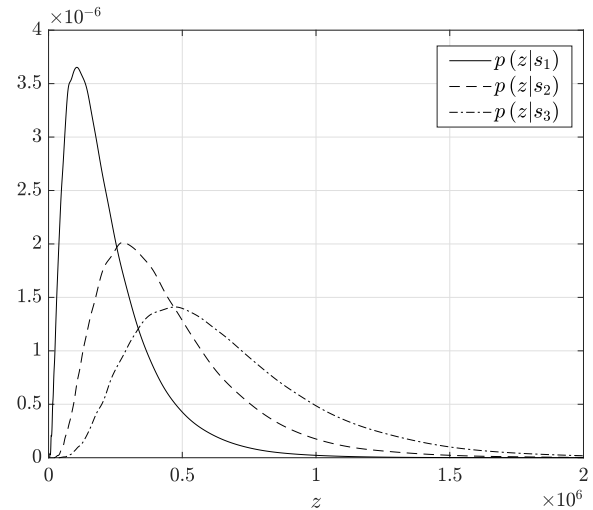
$$p\left(z_u|b_m\right) = \begin{cases} \frac{1}{2^{R|U_u|}\,\Gamma(R|U_u|)}z_u^{R|U_u|-1}\mathrm{e}^{\frac{z_u}{2}}, & m < u, \\[2ex] \frac{\pi\mathrm{e}^{-\frac{z_u}{2}}}{2(R-1)!}\left(\frac{z_u}{2}\right)^{R|U_u|-1}\sum_{j=1}^{J}\left(\prod_{k\neq j}\frac{\frac{1}{\lambda_{u,k}}}{\frac{1}{\lambda_{u,k}}-\frac{1}{\lambda_{u,j}}}\right)G_{1,0:0,2:1,3}^{1,0:2,0:1,0}\left(0\left|\begin{array}{c}-\\R,1\end{array}\right|\begin{array}{c}\frac{1}{2}\\0,1-R|U_u|,\frac{1}{2}\end{array}\right|\frac{1}{\lambda_{u,j}\overline{\gamma}},\frac{z_u}{2}\right), & m \geq u. \end{cases} \quad (32)$$

Test statistics and decision rules: At the receiver, $M-1$ different test statistics are formed for the $M-1$ different subsets of null subcarriers as

$$z_u = \frac{2}{\sigma_w^2}\sum_{r=1}^{R}\sum_{m\in\mathcal{U}_u}|Y_r[m]|^2, \quad u = 1,2,\ldots,M-1, \quad (31)$$

where $\mathcal{U}_u$ is the u-th subset of the in-band null subcarriers. Let $\mathbf{h}_u$ denote the vector comprising the channel coefficients seen by the subcarriers in the u-th subset, $\mathcal{U}_u$, and denote $\{\lambda_{u,j}\}_{j=1}^{J}$, the non-zero eigenvalues of the co-variance matrix $E\left[\mathbf{h}_u\mathbf{h}_u^\dagger\right]$; hence, the distribution of the test statistics, $\{z_u\}_{u=1}^{M-1}$ for different transmitted symbols can be written as in (32).

Then, using the test statistics in (31), a binary decision is made, independently, for each subset to determine whether it contains shifted energy following the same procedure outlined in Section IV.

Let δ_u denote the decision threshold for the u-th null subset and $d_u \in \{0,1\}$ denote the decision made for the u-th null subset, such that d_u is '1' if energy is detected in the u-th subset, i.e. $z_u > \delta_u$, and '0' otherwise. Next, we treat the subset decisions $\{d_u\}_{u=1}^{M-1}$ as the output of a vector communication channel. By this characterization, our problem can be thought of as a traditional detection problem for a general vector channel [44], [45], where the input to the channel is the backscatter symbol, b_m, and the output is the subset decisions, $\{d_u\}_{u=1}^{M-1}$. Hence, if all symbols are equally likely, the optimal decision rule will be the maximum likelihood rule given by

$$\hat{m} = \arg\max_{0\leq m\leq M-1}p\left(\mathbf{d}|b_m\right), \quad (32)$$

where $\mathbf{d} = [d_1 \quad d_2 \quad \cdots \quad d_{M-1}]$ is the $(M-1)$-dimensional binary vector comprising the decisions for all subsets.

Obtaining the exact joint distribution $p\left(d_1, d_2, \ldots, d_{M-1}|b_m\right)$ is mathematically intractable. To simplify analysis, we assume the channel gains are only correlated within a given null subset, but are uncorrelated between different subsets. This assumption will be sufficiently accurate for practical numbers of null subsets and typical values of delay spread as will be shown in Section VI. Thus, the simplified decision rule can be written as

$$\hat{m} = \arg\max_{0\leq m\leq M-1}\prod_{u=1}^{M-1}p\left(d_u|b_m\right), \quad (33)$$

where $p\left(d_u=1|b_m\right) = p\left(z_u\geq\delta_u|b_m\right)$, $p\left(d_u=0|b_m\right) = p\left(z_u<\delta_u|b_m\right)$, and $p\left(z_u|b_m\right)$ is as defined in (32).

Using this decision rule, a decoding function/table that maps the set of possible subset decisions, $\mathcal{D}$, i.e. the set of $(M-1)$-dimensional binary vectors, to the set of the symbols

TABLE I
DECODING TABLE FOR EXAMPLE 1.

Subset Decisions	Symbol Decision
$\mathbf{d}$	$\hat{m}$
$[0\ \ 0\ \ 0], [0\ \ 0\ \ 1]$	0
$[1\ \ 0\ \ 0]$	1
$[0\ \ 1\ \ 0], [1\ \ 1\ \ 0]$	2
$[0\ \ 1\ \ 1], [1\ \ 0\ \ 1], [1\ \ 1\ \ 1]$	3

could be constructed to decode the transmitted backscatter symbol. To elaborate, the decoding table partitions the set of subset decisions, $\mathcal{D}$, into M nonoverlapping subsets, $\{\mathcal{D}_m\}_{m=0}^{M-1}$, such that if $\mathbf{d} \in \mathcal{D}_m$, then $\hat{m} = m$. Table I shows the decoding table for Example 1 following the rule in (33). Note that, although the thresholds used for the binary decisions are a function of the SNR, the decoding function/table for higher-order modulation is not and the same decoding table is used for all SNRs.

Error Analysis: Next, we analyze the error performance of the proposed M-ary backscatter scheme. Assuming all symbols are equally probable, the probability of error can be written as

$$P_e = \frac{1}{M}\sum_{m=1}^{M}P_{e|b_m}, \quad (34)$$

where

$$P_{e|b_m} = P\left[\mathbf{d}\notin\mathcal{D}_m|b_m\right] = \sum_{\mathbf{d}\notin\mathcal{D}_m}p\left(\mathbf{d}|b_m\right). \quad (35)$$

We then make use of the same assumption utilized in the finding the decoding function, namely, that channel gains are only correlated within a given null subset, but are uncorrelated between different subsets. Hence, we can say $p\left(\mathbf{d}|b_m\right) = \prod_{u=1}^{M-1}p\left(d_u|b_m\right)$, where $p\left(d_u|b_m\right)$ can be readily calculated from (14) and (16). Finally, we can write the approximate average probability of error as

$$P_e = \frac{1}{M}\sum_{m=1}^{M}\sum_{\mathbf{d}\notin\mathcal{D}_m}\prod_{u=1}^{M-1}p\left(d_u|b_m\right). \quad (36)$$

VI. RESULTS AND DISCUSSION

In this section, we present simulation results to evaluate the performance of the proposed backscatter modulation scheme and verify the analysis undertaken in previous sections. We study the effects of the maximum channel delay spread, τ, the OFDM symbol size, N_f, and the number of receive antennas, R, on the error performance. We use the scheme in [26] as a baseline for comparison.
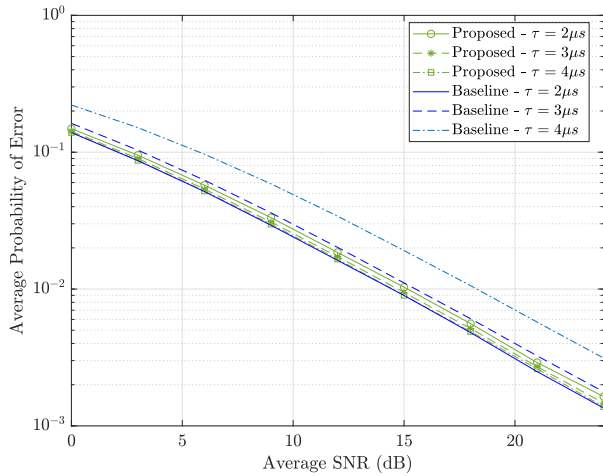
Fig. 4. Average probability of error for different values of maximum channel delay spread. Lines correspond to Monte-Carlo simulations and markers correspond to analytical expressions. Baseline scheme from [26]. $N_f = 1024, N_{cp} = 72, |\mathcal{U}| = 66, L_g = 1$.
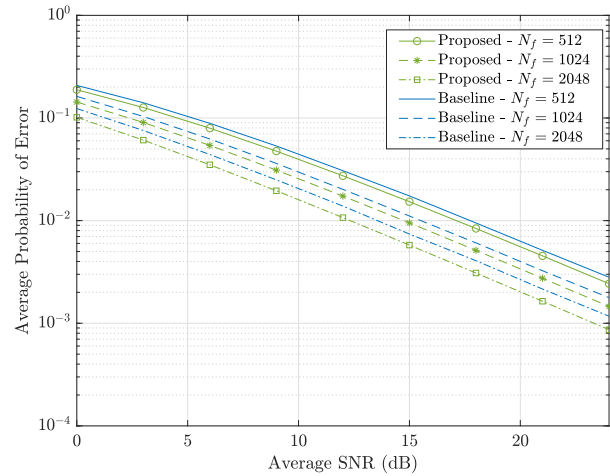

Fig. 5. Average probability of error for different OFDM symbol sizes, and a maximum channel delay spread of $3\mu s$. Lines correspond to Monte-Carlo simulations and markers correspond to analytical expressions. Baseline scheme from [26]. $L_g = 1$.

The scheme in [26] takes advantage of the fact that the portion of the cyclic prefix not affected by the multipath channel, i.e. $n = L, \ldots, N_{cp}$, is repeated in the received signal. The tag waveform is designed to either change its antenna impedance to phase-shift the ambient signal by π for the second part of the OFDM symbol to transmit a '1' bit or keep the phase unchanged to transmit a '0' bit. Let B denote the tag transmitted bit; hence, for $n = L, \ldots, N_{cp}$, we have

$$r[n] \triangleq y[n] - y[n + N_f] = \begin{cases} u[n] + \eta[n], & B = 1, \\ \eta[n], & B = 0, \end{cases} \quad (37)$$

where $y[n]$ is the received signal at the reader, $u[n] = 2g\sqrt{p}\sum_{l=1}^{L_h} s[n-l]h[l]$, and $\eta[n] = w[n] - w[n + N_f]$. Hence, an energy detector can be used to decode the tag information using the test statistics $\frac{1}{\sigma^2}\sum_{L}^{N_{cp}}|r[n]|^2$. Note that the modulation scheme in [26] necessitates that the reader estimate the maximum channel delay spread length L and the scheme fails if this delay spread is equal to the cyclic prefix. Our proposed scheme does not suffer from this limitation.

Suppose the ambient OFDM signal is a 10 MHz LTE carrier [31]; hence, the FFT size is $N_f = 1024$, the "normal" cyclic prefix length is $N_{cp} = 72$, and the number of null subcarriers is 423 of which $|\mathcal{U}| = 66$ are in-band. The maximum channel delay spread, τ is specified in each figure. Fig. 4 compares the average error performance of the proposed scheme to the scheme in [26] for different values of maximum channel delay spread, τ. As expected, the performance of the baseline scheme in [26] deteriorates rapidly as the maximum channel delay spread increases, since the usable part of the cyclic prefix diminishes. On the other hand, the proposed scheme is hardly affected by maximum channel delay spread. Actually, the performance of the proposed scheme slightly improves with increasing delay spread, as the coherence bandwidth decreases and the channel coefficients for the null subcarriers become less correlated. For a delay spread of $4\mu s$, the proposed scheme outperforms the baseline scheme by
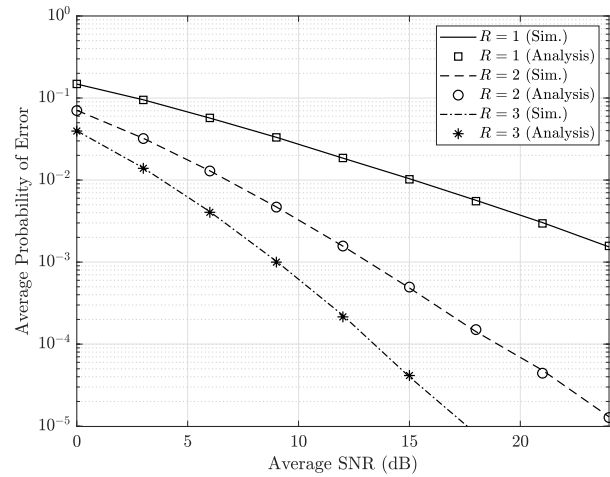
Fig. 6. Average probability of error for different number of receive antennas, $\tau = 3\mu s, N_f = 1024, L_g = 1$.

almost 4 dB at an error rate of 10^{-2}. We also notice that the probability of error from Monte-Carlo simulations coincides with the analytical probability of error, which verifies our analysis.

In Fig. 5, we show the effects of varying the ambient OFDM symbol size on the error performance of the proposed scheme and compare it with the baseline scheme in [26]. We use the LTE OFDM symbol parameters for the 5 MHz, 10 MHz and 20 MHz channel bandwidths [31]. We assume the maximum channel delay spread, τ, is $3\mu s$, which is a typical value in urban outdoor environments. From the figure, increasing the OFDM symbol size improves the performance of both the proposed and baseline schemes; however, the proposed scheme seems to benefit more from increasing the OFDM symbol size. Moreover, for the used typical value of delay spread, the proposed scheme outperforms the baseline scheme for all three OFDM symbol sizes.

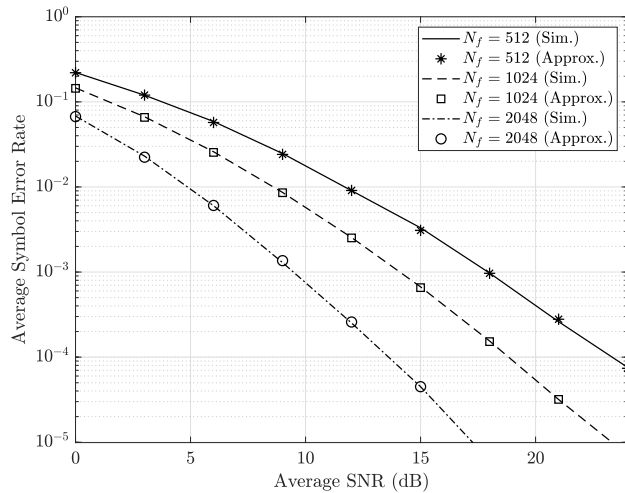Fig. 6 shows the error performance of the multi-antenna

Fig. 7. Average probability of error for the 4-ary backscatter scheme for different ambient OFDM symbol sizes, $R = 4$, $\tau = 3\mu s$, $L_g = 1$.
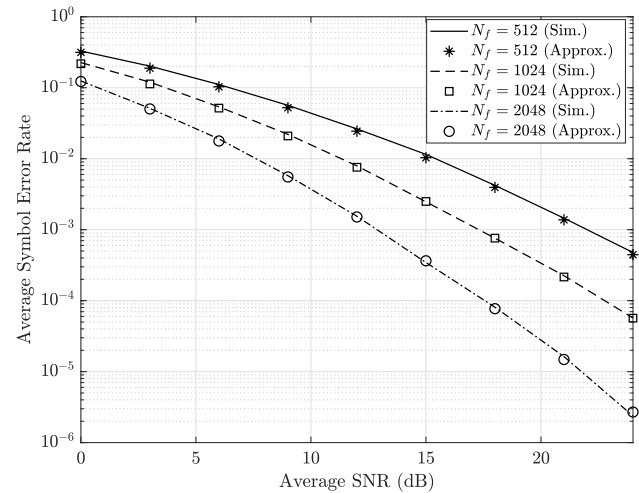

Fig. 9. Average probability of error for the 8-ary backscatter scheme for different ambient OFDM symbol sizes, $R = 8$, $\tau = 3\mu s$, $L_g = 1$.
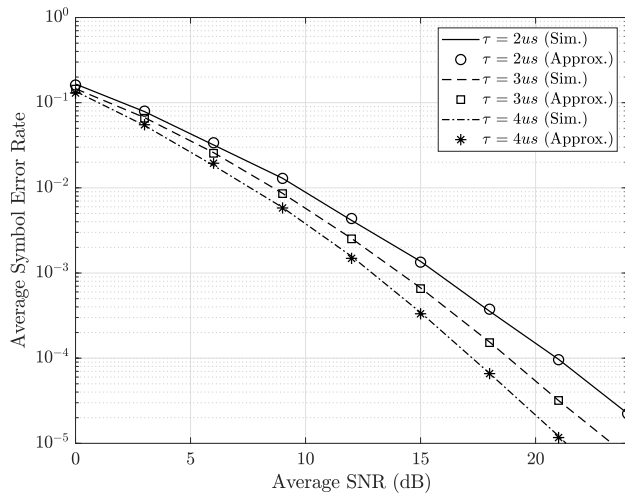

Fig. 8. Average probability of error for the 4-ary backscatter scheme for different values of delay spread, $R = 4$, $N_f = 1024$, $L_g = 1$.
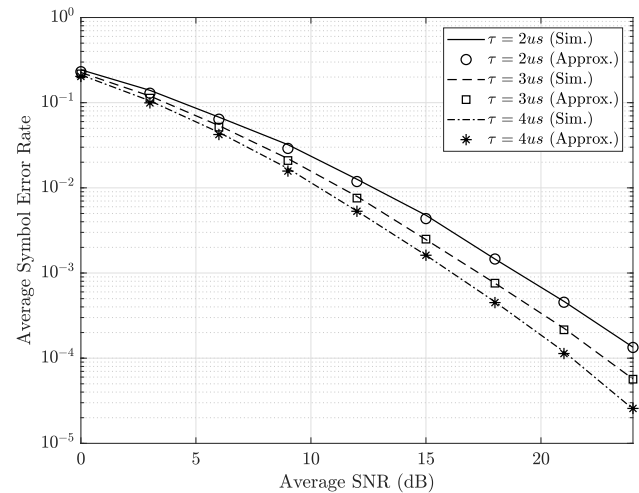

Fig. 10. Average probability of error for the 8-ary backscatter scheme for different values of delay spread, $R = 8$, $N_f = 1024$, $L_g = 1$.

receiver. As we have mentioned earlier, noncoherent post-detection EGC is used since the receiver has no knowledge of the relevant channels or the ambient OFDM symbol. As expected, multiple receive antennas improves the performance dramatically. However, the biggest gain comes from going from a single antenna to two antennas. Increasing the number of antennas to three still gives substantial gain but gains start to diminish as the number of receive antennas increases.

Fig. 7 and Fig. 8 show the performance of the 4-ary scheme designed using the technique in Section V. In Fig. 7, we vary the bandwidth of the ambient OFDM signal while keeping the delay spread and other parameters fixed. As expected, the error performance greatly improves as the bandwidth of the ambient OFDM signal increases since the bandwidth of the in-band null subcarriers, i.e. the guard band, is the directly related to the bandwidth of the ambient OFDM signal. In Fig. 8, we vary the delay spread while keeping the ambient signal bandwidth and other parameters fixed. From

Fig. 8, delay spread seems to have a more pronounced effect on the performance of the 4-ary scheme than on the binary scheme; however, contrary to [26], our scheme seem to benefit greatly from the increasing delay spread.

Finally, Fig. 9 and Fig. 10 show the performance of the 8-ary scheme designed using the technique in Section V. In Fig. 7, we vary the bandwidth of the ambient OFDM signal while keeping the delay spread and other parameters fixed. Similar to the 4-ary case, the error performance greatly improves as the bandwidth of the ambient OFDM signal increases since the bandwidth of the in-band null subcarriers, i.e. the guard band, is the directly related to the bandwidth of the ambient OFDM signal. In Fig. 8, we vary the delay spread while keeping the ambient signal bandwidth and other parameters fixed. Again, similar to 4-ary case, delay spread have a significant impact on the performance of the proposed scheme. Before we conclude this section, note that there is a steep trade-off between tag modulation order and error performance; however, increasing
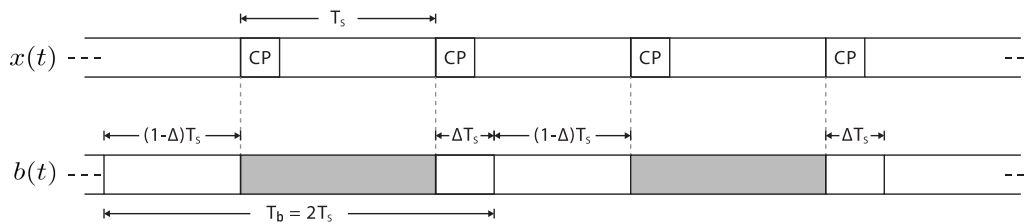
Fig. 11. Timing diagram for asynchronous tag operation. $\Delta \in (0,1)$ denotes where the OFDM symbol overlaps with the tag symbol.

the number of receive antenna could compensate for the loss in performance. For example, for the 4-ary scheme in Fig. 7 and Fig. 8, 4 receive antennas were used, i.e. $R = 4$, while 8 antennas were used for the 8-ary scheme in Fig. 9 and Fig. 10. In all cases, good performance can be obtained with multiple receive antennas and our approximate analysis matches Monte-Carlo simulation results well.

Practical Considerations for Synchronization

Throughout the paper, we assumed a backscatter tag symbol spans one OFDM symbol, which is a common assumption [25], [27]. In the baseline scheme from [25], the authors proposed using traditional correlation techniques at the tag to achieve synchronization. Although ambient OFDM signals usually have well-known standardized reference signals that could be used for synchronization, e.g. preamble (STS and LTS) in WiFi, PSS in LTE and P1 in DVB, synchronization is typically carried out using correlation based techniques in the digital domain. However, these reference signals are typically the most robust part of the ambient signal and the complexity of a simple synchronization receiver designed to detect only the reference signal for timing could be kept reasonable enough for an energy-constrained node, cf. [46]. Moreover, since the reference signals are standardized and well-known, the synchronization operation could also be carried out using specially built analog components and matched filters at the tag.

In general, the proposed scheme is more robust to synchronization errors than the baseline from [25]. In particular, synchronization errors up to the CP length will result in phase rotations in the frequency domain which will not affect our frequency-domain energy detection. This is not the case for the baseline scheme, in which the performance of the system is very sensitive to timing errors as the information transmission is based on perfect synchronization of the system and perfect channel order estimation. Furthermore, in the case synchronization is not achieved between the tag and the OFDM ambient signal, our scheme and analysis would still apply but at a lower rate. In particular, by increasing the tag symbol duration, T_b, to twice the OFDM symbol duration, T_s, we can make sure a full OFDM symbol is subjected to the tag modulation. Fig. 11 shows the timing diagram of asynchronous tag operation, where $\Delta \in (0,1)$ denotes where the OFDM symbol overlaps with the tag symbol. Note that the tag modulation waveform, $b(t)$ is a complex sinusoid and any change in Δ will simply cause a phase shift in the frequency domain that will not affect our energy detection based detector. This will be equivalent to only using every other OFDM symbol. Finally, note that the reader is a traditional wireless receiver and can easily synchronize to the OFDM transmission.

VII. CONCLUSION

We introduced a backscatter modulation technique over ambient OFDM signals. In particular, we took advantage of the null subcarriers found in all OFDM signals and designed the tag modulation waveform such that the backscattered energy lie mostly in the null subcarriers. Hence, an energy detector can be used to detect the backscattered information without requiring knowledge of the ambient OFDM symbol or the relevant channels. This scheme avoids direct link interference since there is no energy from the ambient transmission in the null subcarriers. We have analyzed the error performance of the proposed scheme and provided an exact expression for the error probability in terms of the bivariate Meijer G-function. To improve error performance, we proposed using multiple antennas at the reader and analyzed the error performance in that case. Finally, to improve the communication bit rate, we proposed an M-ary modulation scheme for ambient backscatter that can be decoded noncoherently using only energy detection. Simulation results corroborated our analysis and showed that the proposed scheme outperforms other schemes available in the literature for ambient backscatter over ambient OFDM signals in different scenarios.

APPENDIX A
PROOF OF THEOREM 1

The instantaneous SNR, γ, is a scaled product of two random variables: $|g|^2$, which is an exponential random variable and $q \triangleq \sum_{m \in \mathcal{U}} |H[m]|^2$, which is the sum of $|\mathcal{U}|$ *correlated* exponential random variables. Using the technique in [47], the distribution of q can be found to be

$$f(q) = \sum_{j=1}^{J} \left(\prod_{k \neq j} \frac{\frac{1}{\lambda_k}}{\frac{1}{\lambda_k} - \frac{1}{\lambda_j}} \right) \frac{1}{\lambda_j} e^{-\frac{q}{\lambda_j}}, \qquad (38)$$

where $\{\lambda_j\}_{j=1}^{J}$ are the non-zero eigenvalues of the co-variance matrix $\mathbf{R}_H = E\left[\mathbf{h}\mathbf{h}^\dagger\right]$. Hence, using the product distribution formula [48], we can compute the distribution of the instantaneous SNR, γ, from

$$f(\gamma) = \sum_{j=1}^{J} \left(\prod_{k \neq j} \frac{\frac{1}{\lambda_k}}{\frac{1}{\lambda_k} - \frac{1}{\lambda_j}} \right) \frac{|\mathcal{U}|}{\lambda_j \overline{\gamma}} \int_0^\infty \frac{1}{q} e^{-\left(\frac{q}{\lambda_j} + \frac{|\mathcal{U}|\gamma}{\overline{\gamma}q}\right)} dq,$$
$$(39)$$

where $\overline{\gamma} \triangleq E[\gamma]$ is the average detection SNR. The integral in (39) can be solved with the help of [49, 3.471-9] to yield

$$f(\gamma) = \sum_{j=1}^{J} \left(\prod_{k \neq j} \frac{\frac{1}{\lambda_k}}{\frac{1}{\lambda_k} - \frac{1}{\lambda_j}} \right) \frac{2|\mathcal{U}|}{\lambda_j \overline{\gamma}} \mathbf{K}_0 \left(2\sqrt{\frac{|\mathcal{U}| \, \gamma}{\lambda_j \, \overline{\gamma}}} \right), \quad (40)$$

where $\mathbf{K}_m(\cdot)$ is the modified Bessel function of the second kind and m-th order. Note that the resulting distribution of the instantaneous SNR is actually a mixture of K-distributed random variables [50]. Using the Meijer-G representation of the Bessel function, we arrive at the expression in (11).

APPENDIX B
PROOF OF PROPOSITION 1

To get $p(z|B=1)$, we have to average the noncentral Chi-squared distribution, over the distribution of the instantaneous SNR, γ. This averaging can be written as

$$p(z|B=1) = \int_0^\infty f_{\chi^2}(z; 2|\mathcal{U}|, 2|\mathcal{U}|\gamma) f(\gamma) \, \mathrm{d}\gamma \quad (41)$$

Substituting in the expression for the probability distribution function (PDF) of the noncentral Chi-squared distribution and the expression for the distribution of the SNR from (11), we get

$$p(z|B=1) = \sum_{j=1}^{J} \left(\prod_{k \neq j} \frac{\frac{1}{\lambda_k}}{\frac{1}{\lambda_k} - \frac{1}{\lambda_j}} \right) \int_0^\infty \frac{1}{2\gamma} \, \mathrm{e}^{(z+2|\mathcal{U}|\gamma)/2}$$
$$\times \left(\frac{z}{2|\mathcal{U}|\gamma} \right)^{\frac{|\mathcal{U}|-1}{2}} \mathbf{I}_{|\mathcal{U}|-1} \left(\sqrt{2|\mathcal{U}|\gamma z} \right) \, G_{0,2}^{2,0} \left(\left. \frac{-}{1,1} \right| \frac{|\mathcal{U}| \, \gamma}{\lambda_j \, \overline{\gamma}} \right) \mathrm{d}\gamma \quad (42)$$

where $\mathbf{I}_m(\cdot)$ is the modified Bessel function of the first kind and the m-th order.

Using [51, (07.34.03.0257.01)] to express the Bessel function in terms of the Meijer-G function, and then using [51, (07.34.16.0003.01)] to represent the product of the two Meijer-G function as one bivariate Meijer-G function [40], we can write the integral in (42) as

$$p(z|B=1) = \sum_{j=1}^{J} \pi \left(\prod_{k \neq j} \frac{\frac{1}{\lambda_k}}{\frac{1}{\lambda_k} - \frac{1}{\lambda_j}} \right) \left(\frac{z}{2} \right)^{|\mathcal{U}|-1} \mathrm{e}^{-\frac{z}{2}} \int_0^\infty \gamma^{-1}$$
$$\times \mathrm{e}^{-|\mathcal{U}|\gamma} G_{0,0:0,2:1,3}^{0,0:2,0:1,0} \left(\left. -\left| \frac{-}{1,1} \right| \frac{0, 1-|\mathcal{U}|, \frac{1}{2}}{} \right| \frac{|\mathcal{U}|\gamma}{\lambda_j \overline{\gamma}}, \frac{|\mathcal{U}|z}{2}\gamma \right) \mathrm{d}\gamma, \quad (43)$$

which can be solved using (2.1) from [52] to yield (12).

APPENDIX C
PROOF OF THEOREM 2

The received instantaneous SNR at the output of the combiner, γ_c, is the scaled product of two random vari-

ables: $\sum_{r=1}^{R} |g_r|^2$ with a Gamma distribution, and $q = \sum_{m \in \mathcal{U}} |H[m]|^2$ whose distribution was given in (38) in Appendix A. Using the product distribution formula [48], the SNR distribution at the output of the combiner, γ_c, can be computed from

$$f(\gamma_c) = \sum_{j=1}^{J} \left(\prod_{k \neq j} \frac{\frac{1}{\lambda_k}}{\frac{1}{\lambda_k} - \frac{1}{\lambda_j}} \right) \frac{\gamma_c^{R-1}}{\lambda_j (R-1)! \left(\frac{\overline{\gamma}}{|\mathcal{U}|} \right)^R}$$
$$\times \int_0^\infty \left(\frac{1}{q} \right)^{R-1} \mathrm{e}^{-\left(\frac{q}{\lambda_j} + \frac{|\mathcal{U}|\gamma_c}{\overline{\gamma}q} \right)} \mathrm{d}q, \quad (44)$$

where $\{\lambda_j\}_{j=1}^{J}$ are as defined earlier in (38). The integral in (44) is similar to (39) and can also be solved using [49, 3.471-9] to obtain

$$f(\gamma_c) = \frac{2}{(R-1)!} \sum_{j=1}^{J} \left(\prod_{k \neq j} \frac{\frac{1}{\lambda_k}}{\frac{1}{\lambda_k} - \frac{1}{\lambda_j}} \right) \left(\frac{|\mathcal{U}|\gamma_c}{\lambda_j \overline{\gamma}} \right)^{\frac{R+1}{2}}$$
$$\times \gamma_c^{-1} \mathbf{K}_{R-1} \left(2\sqrt{\frac{|\mathcal{U}|\gamma_c}{\lambda_j \overline{\gamma}}} \right), \quad (45)$$

Using the Meijer G-function representation of the Bessel function, we arrive at (23).

APPENDIX D
PROOF OF PROPOSITION 2

To get $p(z_c|B=1)$, we have to average the noncentral Chi-squared distribution, over the distribution of the instantaneous SNR at the output of the combiner, γ_c. This averaging can be written as

$$p(z_c|B=1) = \int_0^\infty f_{\chi^2}(z_c; 2R|\mathcal{U}|, 2|\mathcal{U}|\gamma_c) f(\gamma_c) \, \mathrm{d}\gamma_c \quad (46)$$

Substituting in the expression for the PDF of the noncentral Chi-squared distribution and the expression for the distribution of the SNR from (23), we get

$$p(z_c|B=1) = \sum_{j=1}^{J} \left(\prod_{k \neq j} \frac{\frac{1}{\lambda_k}}{\frac{1}{\lambda_k} - \frac{1}{\lambda_j}} \right) \int_0^\infty \frac{\gamma_c^{-1}}{2(R-1)!} \mathrm{e}^{\frac{(z+2|\mathcal{U}|\gamma_c)}{2}}$$
$$\left(\frac{z_c}{2|\mathcal{U}|\gamma_c} \right)^{\frac{R|\mathcal{U}|-1}{2}} \mathbf{I}_{R|\mathcal{U}|-1} \left(\sqrt{2|\mathcal{U}|\gamma_c z_c} \right) G_{0,2}^{2,0} \left(\left. \frac{-}{R,1} \right| \frac{|\mathcal{U}|\gamma_c}{\lambda_j \overline{\gamma}} \right) \mathrm{d}\gamma_c. \quad (47)$$

Using [51, (07.34.03.0257.01)] to express the Bessel function in terms of the Meijer-G function, and then using [51, (07.34.16.0003.01)] to represent the product of the two Meijer-G function as one bivariate Meijer-G function [40], we can write the integral in (47) as in (48), which can be solved using (2.1) from [52] to yield (24).

$$p(z_c|B=1) = \sum_{j=1}^{J} \frac{\pi}{2(R-1)!} \left(\prod_{k \neq j} \frac{\frac{1}{\lambda_k}}{\frac{1}{\lambda_k} - \frac{1}{\lambda_j}} \right) \left(\frac{z_c}{2} \right)^{R|\mathcal{U}|-1} \mathrm{e}^{-\frac{z_c}{2}}$$
$$\times \int_0^\infty \gamma_c^{-1} \mathrm{e}^{-|\mathcal{U}|\gamma_c} G_{0,0:0,2:1,3}^{0,0:2,0:1,0} \left(\left. -\left| \frac{-}{R, 1} \right| \frac{0, 1-R|\mathcal{U}|, \frac{1}{2}}{} \right| \frac{|\mathcal{U}|\gamma_c}{\lambda_j \overline{\gamma}}, \frac{|\mathcal{U}|z_c}{2}\gamma_c \right) \mathrm{d}\gamma_c. \quad (48)$$

REFERENCES

[1] C. Boyer and S. Roy, "Backscatter communication and RFID: coding, energy, and MIMO analysis," *IEEE Trans. Commun.*, vol. 62, no. 3, pp. 770–785, Mar. 2014.

[2] D. M. Dobkin, *The RF in RFID, Second Edition: UHF RFID in Practice*, 2nd ed. Newnes, 2012.

[3] V. Liu, A. Parks, V. Talla, S. Gollakota, D. Wetherall, and J. R. Smith, "Ambient backscatter: wireless communication out of thin air," in *Proc. of the ACM SIGCOMM Conf.*, Hong Kong, China, Aug. 2013, pp. 39–50.

[4] B. Kellogg, A. Parks, S. Gollakota, J. R. Smith, and D. Wetherall, "Wi-fi backscatter: internet connectivity for RF-powered devices," in *Proc. of the ACM SIGCOMM Conf.*, Chicago, IL, Aug. 2014, pp. 607–618.

[5] A. N. Parks, A. Liu, S. Gollakota, and J. R. Smith, "Turbocharging ambient backscatter communication," in *Proc. of the ACM SIGCOMM Conf.*, Chicago, IL, Aug. 2014, pp. 619–630.

[6] D. Bharadia, K. R. Joshi, M. Kotaru, and S. Katti, "BackFi: high throughput WiFi backscatter," in *Proc. of the ACM SIGCOMM Conf.*, London, U.K., Aug. 2015, pp. 283–296.

[7] V. Iyer, V. Talla, B. Kellogg, S. Gollakota, and J. R. Smith, "Inter-technology backscatter: towards internet connectivity for implanted devices," in *Proc. of the ACM SIGCOMM Conf.*, Florianópolis, Brazil, Aug. 2016, pp. 356–369.

[8] C. Yang, J. Gummeson, and A. Sample, "Riding the airways: Ultra-wideband ambient backscatter via commercial broadcast systems," in *Proc. IEEE Conf. Computer Commun. (INFOCOM)*, May 2017, pp. 1–9.

[9] R. Duan, R. Jäntti, H. Yigitler, and K. Ruttik, "On the achievable rate of bi-static modulated re-scatter systems," *IEEE Trans. Veh. Technol.*, vol. 66, no. 10, pp. 9609–9613, Oct. 2017.

[10] G. Wang, F. Gao, Z. Dou, and C. Tellambura, "Uplink detection and BER analysis for ambient backscatter communication systems," in *Proc. IEEE Global Commun. Conf. (GLOBECOM)*, San Diego, CA, Dec. 2015.

[11] G. Wang, F. Gao, R. Fan, and C. Tellambura, "Ambient backscatter communication systems: Detection and performance analysis," *IEEE Trans. Commun.*, vol. 64, no. 11, pp. 4836–4846, Nov. 2016.

[12] K. Lu, G. Wang, F. Qu, and Z. Zhong, "Signal detection and BER analysis for RF-powered devices utilizing ambient backscatter," in *Proc. Int. Conf. on Wireless Commun. Signal Process. (WCSP)*, Nanjing, China, Oct. 2015.

[13] Z. Mat, T. Zeng, G. Wang, and F. Gao, "Signal detection for ambient backscatter system with multiple receiving antennas," in *Proc. IEEE 14th Canadian Workshop on Inform. Theory (CWIT)*, St. John's, NL, Canada, Jul. 2015, pp. 50–53.

[14] C. Kang, W. Lee, Y. You, and H. Song, "Signal detection scheme in ambient backscatter system with multiple antennas," *IEEE Access*, vol. 5, pp. 14 543–14 547, Jul. 2017.

[15] J. Qian, F. Gao, and G. Wang, "Signal detection of ambient backscatter system with differential modulation," in *Proc. IEEE Int. Conf. on Acoust., Speech and Signal Process. (ICASSP)*, Shanghai, China, Mar. 2016, pp. 3831–3835.

[16] J. Qian, F. Gao, G. Wang, S. Jin, and H. Zhu, "Semi-coherent detection and performance analysis for ambient backscatter system," *IEEE Trans. Commun.*, vol. 65, no. 12, pp. 5266–5279, Dec. 2017.

[17] Q. Tao, C. Zhong, H. Lin, and Z. Zhang, "Symbol detection of ambient backscatter systems with manchester coding," *IEEE Trans. Wireless Commun.*, vol. 17, no. 6, pp. 4028–4038, Jun. 2018.

[18] J. K. Devineni and H. S. Dhillon, "Ambient backscatter systems: Exact average bit error rate under fading channels," *IEEE Trans. on Green Commun. and Netw., to be published*. [Online]. Available: http://dx.doi.org/10.1109/TGCN.2018.2880985

[19] G. Yang, Q. Zhang, and Y. Liang, "Cooperative ambient backscatter communications for green internet-of-things," *IEEE Internet of Things J.*, vol. 5, no. 2, pp. 1116–1130, Apr. 2018.

[20] Q. Zhang, H. Guo, Y. Liang, and X. Yuan, "Constellation Learning-Based Signal Detection for Ambient Backscatter Communication Systems," *IEEE J. Sel. Areas Commun.*, vol. 37, no. 2, pp. 452–463, Feb. 2019.

[21] G. Yang, D. Yuan, Y. Liang, R. Zhang, and V. C. M. Leung, "Optimal resource allocation in full-duplex ambient backscatter communication networks for wireless-powered IoT," *IEEE Internet of Things J., to be published*. [Online]. Available: http://dx.doi.org/10.1109/JIOT.2018.2872515

[22] X. Liu, Y. Gao, and F. Hu, "Optimal time scheduling scheme for wireless powered ambient backscatter communications in IoT networks," *IEEE Internet of Things J., to be published*. [Online]. Available: http://dx.doi.org/10.1109/JIOT.2018.2889700

[23] D. Darsena, G. Gelli, and F. Verde, "Resource allocation for sensors with wireless power transfer and ambient backscatter transmission," in *2017 Int. Symp. on Wireless Commun. Syst. (ISWCS)*, Aug. 2017, pp. 366–371.

[24] N. V. Huynh, D. T. Hoang, X. Lu, D. Niyato, P. Wang, and D. I. Kim, "Ambient backscatter communications: A contemporary survey," *IEEE Commun. Surveys Tuts.*, vol. 20, no. 4, pp. 2889–2922, May 2018.

[25] G. Yang, Y. C. Liang, R. Zhang, and Y. Pei, "Modulation in the air: Backscatter communication over ambient OFDM carrier," *IEEE Trans. Commun.*, vol. 66, no. 3, pp. 1219–1233, Mar. 2018.

[26] G. Yang and Y. C. Liang, "Backscatter communications over ambient OFDM signals: transceiver design and performance analysis," in *Proc. IEEE Global Commun. Conf. (GLOBECOM)*, Washington, DC, Dec. 2016, pp. 1–6.

[27] D. Darsena, G. Gelli, and F. Verde, "Modeling and performance analysis of wireless networks with ambient backscatter devices," *IEEE Trans. Commun.*, vol. 65, no. 4, pp. 1797–1814, Apr. 2017.

[28] R. Duan, R. Jäntti, M. A. ElMossallamy, Z. Han, and M. Pan, "Multi-antenna receiver for ambient backscatter communication systems," in *Proc. IEEE Workshop on Signal Process. Advances in Wireless Commun. (SPAWC)*, Kalamata, Greece, Jun. 2018, pp. 1–5.

[29] M. A. ElMossallamy, Z. Han, M. Pan, R. Jäntti, K. G. Seddik, and G. Y. Li, "Backscatter communications over ambient ofdm signals using null subcarriers," in *Proc. IEEE Global Commun. Conf. (GLOBECOM), to be published*, Abu Dhabi, UAE, Dec. 2018.

[30] X. Lu, D. Niyato, H. Jiang, D. I. Kim, Y. Xiao, and Z. Han, "Ambient backscatter assisted wireless powered communications," *IEEE Wireless Commun.*, vol. 25, no. 2, pp. 170–177, Apr. 2018.

[31] A. Ghosh, J. Zhang, J. G. Andrews, and R. Muhamed, *Fundamentals of LTE*, 1st ed. Upper Saddle River, NJ: Prentice Hall Press, 2010.

[32] Y. P. E. Wang, X. Lin, A. Adhikary, A. Grovlen, Y. Sui, Y. Blankenship, J. Bergman, and H. S. Razaghi, "A primer on 3gpp narrowband internet of things," *IEEE Commun. Mag.*, vol. 55, no. 3, pp. 117–123, Mar. 2017.

[33] R. Ratasuk, J. Tan, N. Mangalvedhe, M. H. Ng, and A. Ghosh, "Analysis of NB-IoT deployment in LTE guard-band," in *IEEE 85th Veh. Technol. Conf.*, Sydney, Australia, Jun. 2017, pp. 1–5.

[34] H. Urkowitz, "Energy detection of unknown deterministic signals," *Proc. of the IEEE*, vol. 55, no. 4, pp. 523–531, Apr. 1967.

[35] F. W. J. Olver, D. W. Lozier, R. F. Boisvert, and C. W. Clark, Eds., *NIST Handbook of Mathematical Functions*. Cambridge, NY: Cambridge University Press, May 2010.

[36] I. S. Ansari, S. Al-Ahmadi, F. Yilmaz, M. S. Alouini, and H. Yanikomeroglu, "A new formula for the BER of binary modulations with dual-branch selection over generalized-K composite fading channels," *IEEE Trans. Commun.*, vol. 59, no. 10, pp. 2654–2658, Oct. 2011.

[37] H. Chergui, M. Benjillali, and S. Saoudi, "Performance analysis of project-and-forward relaying in mixed MIMO-pinhole and Rayleigh dual-hop channel," *IEEE Commun. Lett.*, vol. 20, no. 3, pp. 610–613, Mar. 2016.

[38] F. F. Digham, M. S. Alouini, and M. K. Simon, "On the energy detection of unknown signals over fading channels," in *Proc. IEEE Int. Conf. on Commun.*, vol. 5, May 2003, pp. 3575–3579.

[39] P. C. Sofotasios, L. Mohjazi, S. Muhaidat, M. Al-Qutayri, and G. K. Karagiannidis, "Energy detection of unknown signals over cascaded fading channels," *IEEE Antennas Wireless Propag. Lett.*, vol. 15, pp. 135–138, 2016.

[40] B. L. Sharma, "On the generalized function of two variables," *Annales de Soc. Sci. de Bruxelles*, no. 79, pp. 26–40, 1965.

[41] H. V. Poor, *An introduction to signal detection and estimation*, 2nd ed. New York, NY: Springer-Verlag New York, Inc., 1994.

[42] M. K. Simon and M.-S. Alouini, *Digital Communication over Fading Channels*, 2nd ed. Wiley-IEEE Press, Dec. 2004.

[43] S. J. Thomas and M. S. Reynolds, "A 96 mbit/sec, 15.5 pJ/bit 16-QAM modulator for UHF backscatter communication," in *Proc. IEEE Int. Conf. on RFID (RFID)*, Orlando, FL, Apr. 2012, pp. 185–190.

[44] H. L. V. Trees, *Detection, Estimation, and Modulation Theory. Part I: Detection, Estimation, and Linear Modulation Theory*, 1st ed. Wiley, 1968.

[45] J. Proakis and M. Salehi, *Digital Communications, 5th Edition*, 5th ed. McGraw-Hill Education, 2007.

[46] H. Tröger, J. Robert, M. Keppeler, M. Hartmann, and A. Heuberger, "Partial OFDM demodulation for frequency synchronization of wireless sensor nodes," in *Int. Symp. on Precision Clock Synchronization for Meas., Control, and Commun. (ISPCS)*, Oct. 2015, pp. 1–6.

This article has been accepted for publication in a future issue of this journal, but has not been fully edited. Content may change prior to final publication. Citation information: DOI 10.1109/TCOMM.2019.2899301, IEEE Transactions on Communications

14

[47] I. S. Ansari, F. Yilmaz, M. S. Alouini, and O. Kucur, "On the sum of gamma random variates with application to the performance of maximal ratio combining over nakagami-m fading channels," in *IEEE 13th Int. Workshop on Signal Process. Advances in Wireless Commun. (SPAWC)*, Cesme, Turkey, Jun. 2012, pp. 394–398.

[48] A. Leon-Garcia, *Probability, Statistics, and Random Processes For Electrical Engineering*, 3rd ed. Pearson, 2008.

[49] I. S. Gradshteĭn and I. M. Ryžik, *Table of Integrals, Series, and Products*, 8th ed., D. Zwillinger, Ed. Academic Press, Oct. 2014.

[50] T. A. Tsiftsis, H. G. Sandalidis, G. K. Karagiannidis, and M. Uysal, "Optical wireless links with spatial diversity over strong atmospheric turbulence channels," *IEEE Trans. Wireless Commun.*, vol. 8, no. 2, pp. 951–957, Feb. 2009.

[51] Wolfram Research Inc., *The Wolfram Functions Site*. [Online]. Available: http://functions.wolfram.com

[52] M. Shah, "On generalizations of some results and their applications," *Collectanea Mathematica*, vol. 24, no. 3, pp. 249–266, 1973.

Karim G. Seddik (S'04-–M'08-–SM'14) is an associate professor in the Electronics and Communications Engineering Department at the American University in Cairo (AUC), Egypt. Before joining AUC, he was an assistant professor in the Electrical Engineering Department at Alexandria University, Egypt. Dr. Seddik received the B.S. (with highest honors) and M.S. degrees in electrical engineering from Alexandria University, Alexandria, Egypt, in 2001 and 2004, respectively. He received his Ph.D. degree at the Electrical and Computer Engineering Department, University of Maryland, College Park 2008. His research interests include cooperative communications and networking, MIMO–OFDM systems, cognitive radio, layered channel coding, and distributed detection in wireless sensor networks. Dr. Seddik has served on the technical program committees of numerous IEEE conferences in the areas of wireless networks and mobile computing. Dr. Seddik is the recipient of the State Incentive Award and Medal of Excellence from the Egyptian government in 2016. Dr. Seddik is a recipient of the Certificate of Honor from the Egyptian President for being ranked first among all departments in College of Engineering, Alexandria University in 2002, the Graduate School Fellowship from the University of Maryland in 2004 and 2005 and the Future Faculty Program Fellowship from the University of Maryland in 2007.

Mohamed A. ElMossallamy (S'14) received the M.Sc. degree in electronics and communications engineering from the American University in Cairo, Cairo, Egypt, in 2017. He is currently pursuing the Ph.D. degree at the Department of Electrical and Computer Engineering, University of Houston, Houston, TX, USA. His current research interests include transceiver design and performance analysis for the Internet of Things, massive MIMO-OFDM systems, and machine learning for wireless communications.

Miao Pan (S'07–M'12–SM'18) received his BSc degree in Electrical Engineering from Dalian University of Technology, China, in 2004, MASc degree in electrical and computer engineering from Beijing University of Posts and Telecommunications, China, in 2007 and Ph.D. degree in Electrical and Computer Engineering from the University of Florida in 2012, respectively. He is now an Assistant Professor in the Department of Electrical and Computer Engineering at University of Houston. He was a recipient of NSF CAREER Award in 2014. His research interests include big data privacy, cybersecurity, cyber-physical systems, and cognitive radio networking. His work won Best Paper Awards in VTC 2018, Globecom 2017 and Globecom 2015, respectively. Dr. Pan is an Associate Editor for IEEE Internet of Things (IoT) Journal from 2015 to 2018. He is a member of ACM and a senior member of IEEE.

Geoffrey Ye Li (S'93-–M'95—SM'97—F'06) received his B.S.E. and M.S.E. degrees in 1983 and 1986, respectively, from the Department of Wireless Engineering, Nanjing Institute of Technology, Nanjing, China, and his Ph.D. degree in 1994 from the Department of Electrical Engineering, Auburn University, Alabama. He was a Teaching Assistant and then a Lecturer with Southeast University, Nanjing, China, from 1986 to 1991, a Research and Teaching Assistant with Auburn University, Alabama, from 1991 to 1994, and a Post-Doctoral Research Associate with the University of Maryland at College Park, Maryland, from 1994 to 1996. He was with AT&T Labs - Research at Red Bank, New Jersey, as a Senior and then a Principal Technical Staff Member from 1996 to 2000. Since 2000, he has been with the School of Electrical and Computer Engineering at Georgia Institute of Technology as an Associate Professor and then a Full Professor. His general research interests include statistical signal processing and machine learning for wireless communications. In these areas, he has published over 500 journal and conference papers in addition to over 40 granted patents. His publications have been cited over 34,000 times and he has been recognized as the *World's Most Influential Scientific Mind*, also known as a *Highly-Cited Researcher*, by Thomson Reuters almost every year. He was awarded *IEEE Fellow* for his contributions to signal processing for wireless communications in 2005. He won 2010 *IEEE ComSoc Stephen O. Rice Prize Paper Award*, 2013 *IEEE VTS James Evans Avant Garde Award*, 2014 *IEEE VTS Jack Neubauer Memorial Award*, 2017 *IEEE ComSoc Award for Advances in Communication*, and 2017 *IEEE SPS Donald G. Fink Overview Paper Award*. He also received 2015 *Distinguished Faculty Achievement Award from the School of Electrical and Computer Engineering, Georgia Tech*. He has been involved in editorial activities for over 20 technical journals for the IEEE, including *founding Editor-in-Chief of IEEE 5G Tech Focus*. He has organized and chaired many international conferences, including *technical program vice-chair of IEEE ICC'03, technical program co-chair of IEEE SPAWC'11, general chair of IEEE GlobalSIP'14, technical program co-chair of IEEE VTC'16 (Spring)* and *general co-chair of IEEE VTC'19 (Fall)*.

Riku Jäntti (M'02 – SM'07) is a Full Professor of Communications Engineering and the head of the department of Communications and Networking at Aalto University School of Electrical Engineering, Finland. He received his M.Sc (with distinction) in Electrical Engineering in 1997 and D.Sc (with distinction) in Automation and Systems Technology in 2001, both from Helsinki University of Technology (TKK). Prior to joining Aalto (formerly known as TKK) in August 2006, he was professor pro tem at the Department of Computer Science, University of Vaasa. Prof. Jäntti is a senior member of IEEE and associate editor of IEEE Transactions on Vehicular Technology. He is also IEEE VTS Distinguished Lecturer (Class 2016). The research interests of Prof. Jäntti include radio resource control and optimization for machine type communications, Cloud based Radio Access Networks, spectrum and co-existence management and quantum communications.

Zhu Han (S'01—M'04–SM'09–F'14) received the B.S. degree in electronic engineering from Tsinghua University, in 1997, and the M.S. and Ph.D. degrees in electrical and computer engineering from the University of Maryland, College Park, in 1999 and 2003, respectively.

From 2000 to 2002, he was an R&D Engineer of JDSU, Germantown, Maryland. From 2003 to 2006, he was a Research Associate at the University of Maryland. From 2006 to 2008, he was an assistant professor at Boise State University, Idaho. Currently, he is a Professor in the Electrical and Computer Engineering Department as well as in the Computer Science Department at the University of Houston, Texas. His research interests include wireless resource allocation and management, wireless communications and networking, game theory, big data analysis, security, and smart grid. Dr. Han received an NSF Career Award in 2010, the Fred W. Ellersick Prize of the IEEE Communication Society in 2011, the EURASIP Best Paper Award for the Journal on Advances in Signal Processing in 2015, IEEE Leonard G. Abraham Prize in the field of Communications Systems (best paper award in IEEE JSAC) in 2016, and several best paper awards in IEEE conferences. Currently, Dr. Han is an IEEE Communications Society Distinguished Lecturer.